Pergamon

PII: S0021-8502(99)00576-5

www.elsevier.com/locate/jaerosci

J. Aerosol Sci. Vol. 31, No. 10, pp. 1129–1144, 2000

Printed in Great Britain
0021-8502/00/$ - see front matter

THE SCANNING FLOW DMA

Don R. Collins, Athanasios Nenes, Richard C. Flagan* and John H. Seinfeld

Department of Chemical Engineering, California Institute of Technology, MC-210-41, Pasadena, CA 91125, USA

(*First received* 25 *February* 1999; *and in final form* 3 *December* 1999)

Abstract—A new method of DMA operation has been implemented in which the flow rates are continuously changed in conjunction with the applied voltage. By optimizing the flow and voltage ramps, improvements can be made in the DMA's measurable size range, counting statistics, resolution, or a partial combination of each of these. Detailed modeling of this technique suggests that errors on the order of 2 to 5% result from incorrect assumptions concerning the flow profile within the DMA. The experimental system enabled accurate control of flows that were varied by an order of magnitude in as little as 30 s. Excellent agreement was obtained between mobility distributions recovered from a voltage ramp, a flow ramp, and a combined voltage and flow ramp. Slight deviations were apparent in the recovered data as the flow scan time was reduced from 60 to 30 s. © 2000 Elsevier Science Ltd. All rights reserved.

1. INTRODUCTION

The differential mobility analyzer (DMA) consists of a pair of parallel electrodes between which a potential is applied and a gas flows. An aerosol flow, Q_a, containing charged particles is introduced adjacent to one of the electrodes. A particle-free sheath flow, Q_{sh}, initially separates the aerosol flow from the opposite electrode. A voltage applied to one of the electrodes (typically the center rod of a coaxial cylinder classifier) produces an electric field that causes charged particles to migrate toward the opposite electrode as they are carried through the classifier by the gas flow. Particles that migrate across the gap between the two electrodes in the time they are carried from the upstream aerosol inlet to a downstream exit port are discharged in a small classified sample flow, Q_s. Other particles either deposit on the electrode surfaces, or exit the classifier in the excess flow, Q_e. The particles contained in the outlet sample flow are classified in terms of electrical mobility, Z_p, which is defined as the migration velocity per unit field strength. The relationship between particle transmission efficiency and particle mobility is referred to as the transfer function, $\Omega(Z_p)$. The transmitted particles have mobilities distributed in a narrow region about Z_p^*, commonly labeled the centroid mobility because of the symmetry of that distribution for large particles. For a DMA operated with constant flow rates and voltage, the centroid mobility can be expressed as (Knutson and Whitby, 1975; Zhang *et al.*, 1995)

$$Z_p^* = \alpha \frac{2Q_{sh} + Q_a - Q_s}{V} \tag{1}$$

where α is a function only of the geometry of the DMA, and V is the applied voltage. This expression applies to both cylindrical and radial DMAs. The classified particle diameter, D_p, can then be inferred from the electrical mobility through

$$\frac{D_p}{C_c(D_p)} = \frac{ie}{3\pi\mu Z_p} \tag{2}$$

where i is the number of elementary charges on the particle, e is the elementary unit of charge, and $C_c(D_p)$ is the slip correction factor for a particle of diameter D_p.

* Author to whom all correspondence should be addressed.

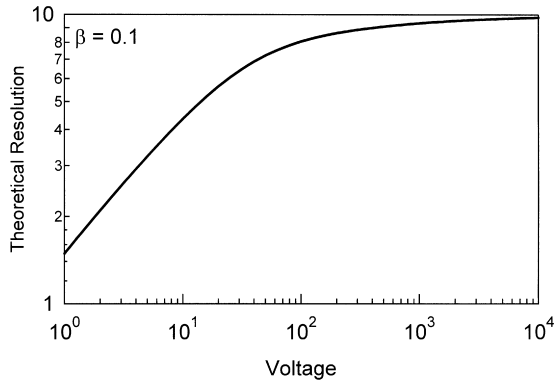

Fig. 1. Limiting DMA resolution for a typical cylindrical DMA with an aerosol to sheath flow ratio of 0.1.

By monitoring the classified sample flow with a continuous-flow particle detector and making a series of measurements at different applied field strengths, the particle size distribution of the aerosol being sampled can be inferred. Utilization of a computer to step the applied voltage and simultaneously record particle counts made the DMA a practical instrument for measuring size distributions (Fissan *et al*., 1983; Brink *et al*., 1983). Continuous scanning of the applied voltage reduced the size distribution measurement time from the many minutes required for stepping-mode measurements to under one minute (Wang and Flagan, 1989). Further enhancement by continuously monitoring the volumetric flow rates of all four streams entering and leaving the DMA, combined with active flow control to maintain the desired flows in spite of pressure variations, has made the DMA a robust system suitable for airborne measurements (Russell *et al*., 1996).

The computer-controlled DMA fills a very important niche in aerosol particle characterization, allowing high resolution size distribution measurements of particles below the range of optical particle counters and aerodynamic particle sizers, spanning the range from 1 μm to 3 nm or less. While DMA measurements can be made over a broad range of particle sizes, the size range that can be covered in a given measurement scenario is constrained by practical limits on the range of voltages that can be scanned. The highest classification voltages must be below the threshold for electrostatic breakdown, or spurious counts will be recorded, and the instrument may be damaged. This threshold decreases with decreasing gas density according to Paschen's Law (Meek and Craggs, 1978), complicating aircraft and other low pressure applications. At the opposite extreme, particle diffusion results in deterioration of the instrumental resolution as the voltage is decreased below a threshold value (Stolzenburg, 1988; Flagan, 1999). Figure 1 presents the relationship between limiting resolution and applied voltage for the TSI 3071 cylindrical DMA operated with an aerosol to sheath flow ratio, β, of 10. To some degree, the operator must, therefore, decide whether to focus measurements on the fine particle end of the size spectrum, or to measure larger particles. Additional constraints exist on the flow rates that can be accurately employed. While limits vary between DMAs, sample flow rates below 0.1–0.2 L min^{-1} will typically result in poor counting statistics; for the commonly used TSI 3071 cylindrical DMA, a sheath flow rate of 20 L min^{-1} will be associated with a Reynold's Number of 960, approaching the point at which flow instabilities may occur, although carefully designed and fabricated instruments have been successfully operated well beyond this point (de Juan and de la Mora, 1998). Techniques used to extend the achievable size range in DMA measurements include use of multiple DMAs operated in parallel (Flagan *et al*., 1991), and switching a single instrument between high and low flow rate modes (Hansson, 1997).

This paper will demonstrate a new approach to extending the range of size distribution measurements attainable with a single DMA while maintaining the short measurement times that are possible with the scanning mode. By simultaneously scanning both the DMA voltage and flow rates, the particle size range can be dramatically extended while, at the

same time, improving both the limiting size resolution and counting statistics associated with the measurement.

2. SCANNING FLOW DMA OPERATION

When particles are classified using a DMA operated at constant voltage and constant flow rates, all transmitted particles follow similar trajectories in the absence of diffusion. Using a particle stream function analysis, the transmission characteristics of the DMA can be shown to be independent of the details of the gas flow velocity profile. If either the voltage or flow rates is allowed to vary, a particle stream function analysis is no longer possible, and examination of particle equations of motion is necessary. In its most general form, particle velocity is described by

$$\frac{\mathrm{d}x}{\mathrm{d}t} = Z_{\mathrm{p}}E_x + u(x,r,t), \tag{3}$$

$$\frac{\mathrm{d}r}{\mathrm{d}t} = Z_{\mathrm{p}}E_r + v(x,r,t), \tag{4}$$

where E_x and E_r are the electric field vectors in the x and r directions, respectively, and $u(x,r,t)$ and $v(x,r,t)$ are the gas flow velocities in the x and r directions, respectively. For the theoretical and experimental analyses presented here, a cylindrical DMA with dimensions similar to those of the TSI 3071 will be considered. Therefore, the following expressions are derived for a cylindrical DMA, although similar expressions exist for a radial DMA. Particles are introduced along the outer electrode in the DMA, radius R_2, and migrate toward the inner one, radius R_1. For a properly designed cylindrical DMA, the electric field in the annular gap between these electrodes is

$$E_x \simeq 0 \quad \text{and} \quad E_r = \frac{V}{r\ln(R_1/R_2)}. \tag{5}$$

The particle velocity must be known throughout its residence time in the DMA to determine the efficiency with which particles of specified mobility are classified. This task is greatly simplified if all sampled particles follow the same trajectories, i.e. $\mathrm{d}r/\mathrm{d}x \neq f(t)$. The residence time of a classified particle then varies only with the average gas flow rate during its transit in the DMA. If the flow rate variation does not change the relative flow profile within the DMA, e.g. if the flow is fully developed, the particle velocity would be given by

$$\frac{\mathrm{d}x}{\mathrm{d}t} = u_0(x,r)\frac{Q(t)}{Q_0}, \tag{6}$$

$$\frac{\mathrm{d}r}{\mathrm{d}t} = \frac{Z_{\mathrm{p}}V(t)}{r\ln(R_1/R_2)} + v_0(x,r)\frac{Q(t)}{Q_0}, \tag{7}$$

$$\frac{\mathrm{d}r}{\mathrm{d}x} = \frac{Z_{\mathrm{p}}Q_0}{ru_0(x,r)\ln(R_1/R_2)}\frac{V(t)}{Q(t)} + \frac{v_0(x,r)}{u_0(x,r)}. \tag{8}$$

2.1. *Voltage scan at constant flow rate*

In the first report of scanning DMA operation, Wang and Flagan (1989) utilized an exponential voltage ramp while maintaining constant flow rates to accelerate the measurement of complete size distributions. The particle equations of motion for this voltage-scanning DMA are

$$\frac{\mathrm{d}x}{\mathrm{d}t} = u_0(x,r), \tag{9}$$

$$\frac{\mathrm{d}r}{\mathrm{d}t} = \frac{Z_\mathrm{p} V_0}{r \ln(R_1/R_2)} \mathrm{e}^{\pm t/\tau} + v_0(x,r), \tag{10}$$

$$\frac{\mathrm{d}r}{\mathrm{d}x} = \frac{Z_\mathrm{p} V_0}{r u_0(x,r) \ln(R_1/R_2)} \mathrm{e}^{\pm t/\tau} + \frac{v_0(x,r)}{u_0(x,r)}. \tag{11}$$

Breaking the time, t, into the time a particle has spent in the DMA, Δt, and the time at which the particle entered the DMA, t_in, and integrating the radial velocity over time yields

$$r^2 = R_\mathrm{in}^2 + \frac{2 Z_\mathrm{p} V_0(\pm\tau)}{\ln(R_1/R_2)} \mathrm{e}^{\pm t_\mathrm{in}/\tau} (\mathrm{e}^{\pm \Delta t/\tau} - 1) + \int_{t_\mathrm{in}}^{t_\mathrm{in}+\Delta t} r v_0(x,r) \mathrm{d}t \tag{12}$$

where R_in is the radial position of the particle upon entering the DMA. If, as desired, all sampled particles follow the same trajectory,

$$\int_{t_\mathrm{in}}^{t_\mathrm{in}+\Delta t} r v_0(x,r) \mathrm{d}t = f(x,r) \quad \text{and} \quad \int_{t_\mathrm{in}}^{t_\mathrm{in}+t_\mathrm{res}} r v_0(x,r) \mathrm{d}t = k = \text{constant} \tag{13}$$

where t_res is the transit time a classified particle will take to migrate to radial position R_out. Solution of equation (12) with these limits of integration provides a relationship between the mobility of a classified particle and the time at which it entered the DMA

$$Z_\mathrm{p} = \pm \frac{V_0(R_\mathrm{out}^2 - R_\mathrm{in}^2 - k)}{2\tau \ln(R_1/R_2)} \frac{1}{\mathrm{e}^{\pm t_\mathrm{in}/\tau}(\mathrm{e}^{\pm t_\mathrm{res}/\tau} - 1)}. \tag{14}$$

The characteristic mobility of the classified particles leaving the DMA at any instant of time is generally taken as that of the particle that entered the DMA at the centroid of the incoming aerosol flow (expressed here as the radial position R_in), and exits at the centroid of the outgoing classified sample flow at R_out. The median mobility, $Z_\mathrm{p}^\mathrm{med}$, of the transmitted particles (and the transfer function) is, however, more relevant to ultimate inversion of the data. Substitution of equation (14) into equations (11) and (12) gives

$$\frac{\mathrm{d}r}{\mathrm{d}x} = \pm \frac{R_\mathrm{out}^2 - R_\mathrm{in}^2 - k}{2\tau r u_0(x,r)} \frac{\mathrm{e}^{\pm \Delta t/\tau}}{\mathrm{e}^{\pm t_\mathrm{res}/\tau} - 1} + \frac{v_0(x,r)}{u_0(x,r)}, \tag{15}$$

$$r^2 = R_\mathrm{in}^2 + (R_\mathrm{out}^2 - R_\mathrm{in}^2 - k) \frac{\mathrm{e}^{\pm \Delta t/\tau} - 1}{\mathrm{e}^{\pm t_\mathrm{res}/\tau} - 1} + f(x,r). \tag{16}$$

Finally, solving equation (16) for $\mathrm{e}^{\pm \Delta t/\tau}$ and substituting this relationship back into equation (15) yields a time-independent expression for the particle trajectory, i.e.,

$$\frac{\mathrm{d}r}{\mathrm{d}x} = \pm \frac{1}{u_0(x,r)} \left(\frac{R_\mathrm{out}^2 - R_\mathrm{in}^2 - k}{2\tau r (\mathrm{e}^{\pm t_\mathrm{res}/\tau} - 1)} + \frac{r^2 - R_\mathrm{in}^2 - f(x,r)}{2\tau r} \right) + \frac{v_0(x,r)}{u_0(x,r)}. \tag{17}$$

The result is a transfer function that maintains a constant shape throughout a scan, and for which the centroid and median mobilities vary with $\mathrm{e}^{\pm t/\tau}$. This simplifies the analysis of voltage-scanning DMA data, but imposes constraints on the manner in which voltage is varied. Additionally, only those particles that experience the voltage ramp throughout their entire transit are considered, i.e. particles that enter prior to the start of the ramp or exit the column after the ramp is complete are not accurately described by this first-order model. Relative to stepping mode operation, this restriction reduces the mobility range analyzed to

$$\frac{(Z_{\mathrm{p}_\mathrm{max}}/Z_{\mathrm{p}_\mathrm{min}})_\mathrm{scan}}{(Z_{\mathrm{p}_\mathrm{max}}/Z_{\mathrm{p}_\mathrm{min}})_\mathrm{step}} = \frac{(\bar{V}_\mathrm{max})_\mathrm{scan}}{V_\mathrm{max}} \frac{V_\mathrm{min}}{(\bar{V}_\mathrm{min})_\mathrm{scan}} = \frac{\int_0^{t_\mathrm{res}} \mathrm{e}^{-t/\tau} \mathrm{d}t}{t_\mathrm{res}} \frac{t_\mathrm{res}}{\int_0^{t_\mathrm{res}} e^{t/\tau} \mathrm{d}t} \tag{18}$$

$$= -\frac{(V_\mathrm{max}/V_\mathrm{min})^{-t_\mathrm{res}/t_\mathrm{scan}} - 1}{(V_\mathrm{max}/V_\mathrm{min})^{t_\mathrm{res}/t_\mathrm{scan}} - 1} = \left(\frac{V_\mathrm{min}}{V_\mathrm{max}} \right)^{t_\mathrm{res}/t_\mathrm{scan}}. \tag{19}$$

For a TSI 3071 DMA operated with a sheath flow rate of 3 L min^{-1}, a 60 s scan over 3 decades of voltage reduces the analyzed mobility range by a factor of approximately 2.4.

Although the shape of the DMA transfer function does not change during an exponential voltage scan, it may differ from that in the constant voltage case due to differences in the time that the particle resides in different regions of the flow. At constant voltage, the particle residence time equals the mean fluid residence time. When the voltage increases with time, a particle will pass through the low velocity, low field region near the outer electrode more slowly than it will through the high velocity core of the flow or the high field, low velocity region adjacent to the inner electrode. The reverse is true for a decreasing voltage scan. This leads to an asymmetry in the transfer function and a shift in the median mobility of the two scans. The effect is generally small at commonly used scan rates, but the scanning DMA system should be calibrated to eliminate the resulting biases. As a first approximation, the median mobility can be estimated using equation (14) with the assumption that the particle residence time is the same as the mean gas residence time. By measuring the system response to a monodisperse aerosol and adjusting the so-called plumbing time until the recovered distribution is consistent with the known size of the sampled aerosol particles, the system can be calibrated for future measurements. For plug flow, this plumbing time is simply the transit time between the DMA outlet and the detector, but when the gas velocity varies with position, it is the sum of the transit time and an adjustment that accounts for the difference between the residence time of a sampled particle, and that of the mean gas flow. From equation (14), this adjustment time, t', is related to the (unknown) particle residence time, t_{res_p}, through

$$(\exp(\pm t_{\mathrm{res}_p}/\tau) - 1)\exp(\pm t_{\mathrm{in}}/\tau) = (\exp(\pm t_{\mathrm{res}_g}/\tau) - 1)\exp(\pm (t_{\mathrm{in}} + t')/\tau)$$

or

$$t' = \pm \tau \ln \frac{\exp(\pm t_{\mathrm{res}_p}/\tau) - 1}{\exp(\pm t_{\mathrm{res}_g}/\tau) - 1}. \tag{20}$$

Even if the particle residence time during an up scan is the same as that during a down scan, this adjustment will not be, so two plumbing times must be determined.

2.2. *Flow and voltage scan*

Even with the limitations and uncertainties associated with the exponential voltage-scanning technique, the time-independent transfer function is preferable to the time-varying transfer function that would result from other voltage ramps. Therefore, for a flow-scanning DMA, it would be desirable to find a suitable set of ramps that would satisfy the constant trajectory requirement discussed above. From equation (8), it is clear that, if $V(t)/Q(t) = \text{constant}$, $\mathrm{d}r/\mathrm{d}x \neq f(t)$ provided the velocity profile in the DMA does not change, and calculation of the DMA transfer function will be facilitated. However, contrary to this requirement, an increasing voltage must be coupled with decreasing flow rates and vice versa to expand the measurable size range. Unfortunately, no ramp combinations exist that satisfy both of these requirements. Moreover, unless the variation is slow and the flow is fully developed throughout the scan, the assumption that the shape of the flow profile remains constant is unrealistic when flow rates are varied. Thus, although flow-scanning increases the dynamic range of the DMA, it may complicate data analysis since the transfer function will vary with time, as will the flow profile within the DMA.

The flow in a DMA is usually approximated either as a plug flow in which the gas velocity is uniform across the flow channel, or as a fully developed laminar flow in which the velocity varies transverse to the flow, but not in the streamwise direction (at least for the cylindrical DMA). For operation at constant flow rate and field strength, these flows represent extremes that bound the actual performance. Since scanning operation may be more sensitive to the details of the velocity profile, we have examined the impact of deviations

from these idealized flow fields on two measures of instrument response: (i) the integral of the transfer function over the logarithm of the mobility,

$$I_{\log Z} = \int_{-\infty}^{\infty} \Omega\left(\log \frac{Z_p}{Z_{p_0}}\right) \mathrm{d} \log \frac{Z_p}{Z_{p_0}};$$

and (ii) the median mobility of the transfer function, Z_p^{med}, defined such that

$$\int_{-\infty}^{\log Z_p^{med}/Z_{po}} \Omega\left(\log \frac{Z_p}{Z_{p_0}}\right) \mathrm{d} \log \frac{Z_p}{Z_{p_0}} = \frac{1}{2} \int_{-\infty}^{\infty} \Omega\left(\log \frac{Z_p}{Z_{p_0}}\right) \mathrm{d} \log \frac{Z_p}{Z_{p_0}}. \tag{21}$$

For a size distribution that is broad compared to the transfer function, $I_{\log Z}$ is proportional to the particle transmission rate.

The flow field within the DMA was predicted by numerically solving the Navier–Stokes equations for laminar flow (Bird *et al*., 1960) using a finite volume method (Patankar, 1980). A staggered grid, in which each velocity grid node lies between two volumes, is used for the calculations (Patankar, 1980). This procedure ensures that the numerical solution yields a realistic pressure field. The SIMPLE iterative solution method is used to solve the finite volume equations (Patankar, 1980). The computer code used for the numerical simulations is a modified version of the TEACH-2E code (Gosman and Pun, 1974). For each flow rate considered, the numerical solution was obtained using 150 cells for the x- and 50 cells for the r-directions, respectively. For the theoretical and experimental analyses presented in this paper, the sheath flow rate was varied between 2 and 20 L min^{-1}, while the sheath to aerosol flow rate ratio was maintained at 10. The calculated velocity vectors and fluid streamlines corresponding to the extremes within this range are shown in Fig. 2. While differences do exist between the 2 and 20 L min^{-1} flow fields, they are seen to be significant only immediately downstream of the aerosol inlet and immediately upstream of the sample outlet. The fastest flow ramp considered, 30 s, is long enough compared to the characteristic

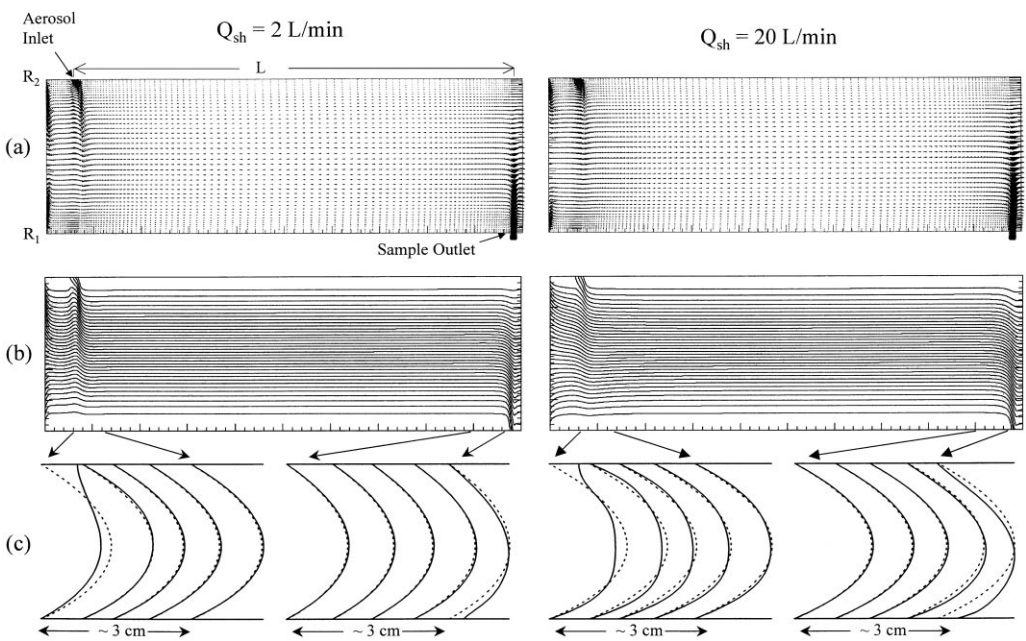

Fig. 2. (a) Modeled velocity vectors, (b) modeled fluid streamlines, and (c) deviations between modeled (solid line) and fully developed (dashed line) flow profiles near the inlet and outlet of a cylindrical DMA with overall dimensions identical to the TSI 3071. The two cases given (2 and 20 L min^{-1}) represent the extremes employed in our analysis. For both cases, a sheath to aerosol flow rate ratio of 10 is used.

time for viscous diffusion ($\tau_v \sim (R_{in}^2 - R_{out}^2)/v \sim 5$ s) that the flow may be assumed to be quasi-steady.

The transfer function was examined for scans with a sheath flow rate variation between 2 and 20 L min^{-1}, and a voltage range of 10 V to 10,000 V. Since the perturbations caused by scanning DMA operations depend on the rate of change of the flow and voltage, and the variations of these parameters span the majority of the accessible ranges for the TSI long column cylindrical DMA (Model 3071 or 3081), the analysis that follows provides an estimate of the maximum perturbations that are likely for scans as short as 30 s. For plug flow, the axial particle velocity is constant and equals the mean gas velocity. For this simplified case, the voltage-scanning transfer function that was presented by Wang and Flagan can be used for combined flow and voltage-scanning operation with little modification,

$$\Omega(Z_p, t) = \max\{0, \min[(K(t) + 1 - 1/\beta), (-K(t) + 1 + 1/\beta)]\} \quad (\text{for } Q_a = Q_s), \tag{22}$$

where

$$K(t) = -Z_p \frac{2\pi L}{\beta \ln(R_1/R_2)} \frac{\int_{t-t_{res}}^{t} V(t')\mathrm{d}t'}{\int_{t-t_{res}}^{t} Q_{sh}(t')\mathrm{d}t'}. \tag{23}$$

To clearly show the increasing transmission rate of particles with increasing flow rate, an effective transfer function, $\Omega'(Z_p, t)$, is defined as the product of the transmission efficiency and sample flow rate normalized to its initial value,

$$\Omega'(Z_p, t) = \Omega(Z_p, t) \frac{Q_s(t)}{Q_s(t=0)}. \tag{24}$$

For plug flow, the integral of this expression over the logarithm of mobility varies only with sample flow rate, while the median mobility is directly related to the mean voltage and flow rates experienced over the gas residence time, i.e.

$$\int_{-\infty}^{\infty} \Omega\left(\log \frac{Z_p}{Z_{p_0}}\right) \mathrm{d} \log \frac{Z_p}{Z_{p_0}} = C_1 \frac{Q_s(t)}{Q_s(t=0)}, \tag{25}$$

$$Z_p^{med} = C_2 \frac{\int_{t-t_{res}}^{t} V(t')\mathrm{d}t'}{\int_{t-t_{res}}^{t} Q_{sh}(t')\mathrm{d}t'}, \tag{26}$$

where C_1 and C_2 are constants related to β and the DMA dimensions. For both modeled and fully developed flow, $I_{\log Z}$ and Z_p^{med} were calculated by numerically integrating particle trajectories over time. The transfer functions calculated using the modeled flow fields for a 60 s ramp are shown in Fig. 3. Following the convention given by Wang and Flagan (1989), voltage is increased (while flow rate is decreased) during an up scan (decreasing mobility) and decreased (while flow rate is increased) during a down scan (increasing mobility). The direct relationship between sample flow rate and transfer function height is apparent. Figure 4 shows the integral and median mobility of the transfer function as a function of time for this 60 s scan, along with the corresponding quantities for the plug and fully developed flow cases. Consistent with the use of the time offset described in the analysis of voltage-scanning data, the median mobility curves were shifted with respect to time (0.45 s) to achieve agreement. While slight deviations are seen to exist between the three cases considered, they are relatively small, with maximum errors in both $I_{\log Z}$ and Z_p^{med} of approximately 2 and 6% for the developed and plug flow cases, respectively. The relationships between these maximum discrepancies and scan time are presented in Fig. 5. Fully developed flow better approximates the actual performance of the DMA than does plug flow. The deviations in median mobility resulting from the fully developed flow model increase slightly with decreasing scan times. Although these errors may be excessive for certain applications, they are of comparable magnitude to other errors common in size distribution measurements such as those related to charging probability uncertainty and flow control.

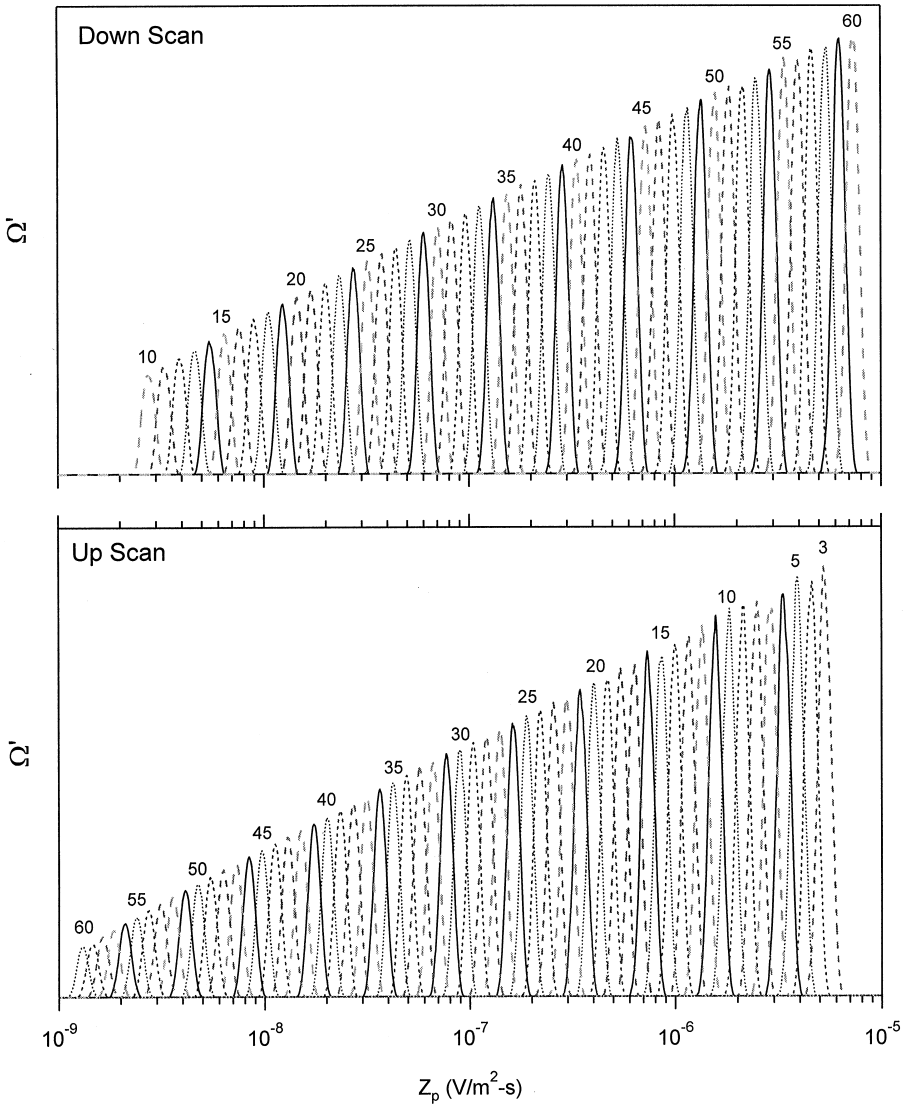

Fig. 3. DMA transfer functions calculated using modeled flow fields for a 60 s scan during which the sheath flow was varied linearly from 2 to 20 L min^{-1} as the voltage was ramped from 10 to 10,000 V. To clearly show the variation in the transfer functions as a function of flow rate, only those for which particles experienced ramping flows and voltage throughout their transit are shown.

One further complication arising from this method is the pressure variation within the DMA that is caused by flow rate dependent finite pressure drops in the entrance and exit regions of the DMA and across the laminar flow elements that are used to monitor the flow rates. This leads to a slight imbalance in the flow rates since the density within the column will change in the course of the measurements. The pressure drop within the classification region of the DMA is small, so impacts of the pressure drops can be examined by considering a mole balance on the DMA column. The accumulation of material within the DMA can be expressed as the difference between the incoming and outgoing flows, i.e.

$$\left(\frac{dc}{dt}\right)_{DMA} = \frac{c(Q_a + Q_{sh} - Q_s - Q_e)}{\mathcal{V}_{DMA}}, \tag{27}$$

where c is the molar concentration of the gas within the DMA and $\mathcal{V}_{DMA}$ is the volume of the DMA. As will be described below, the sheath and excess air flows are connected through

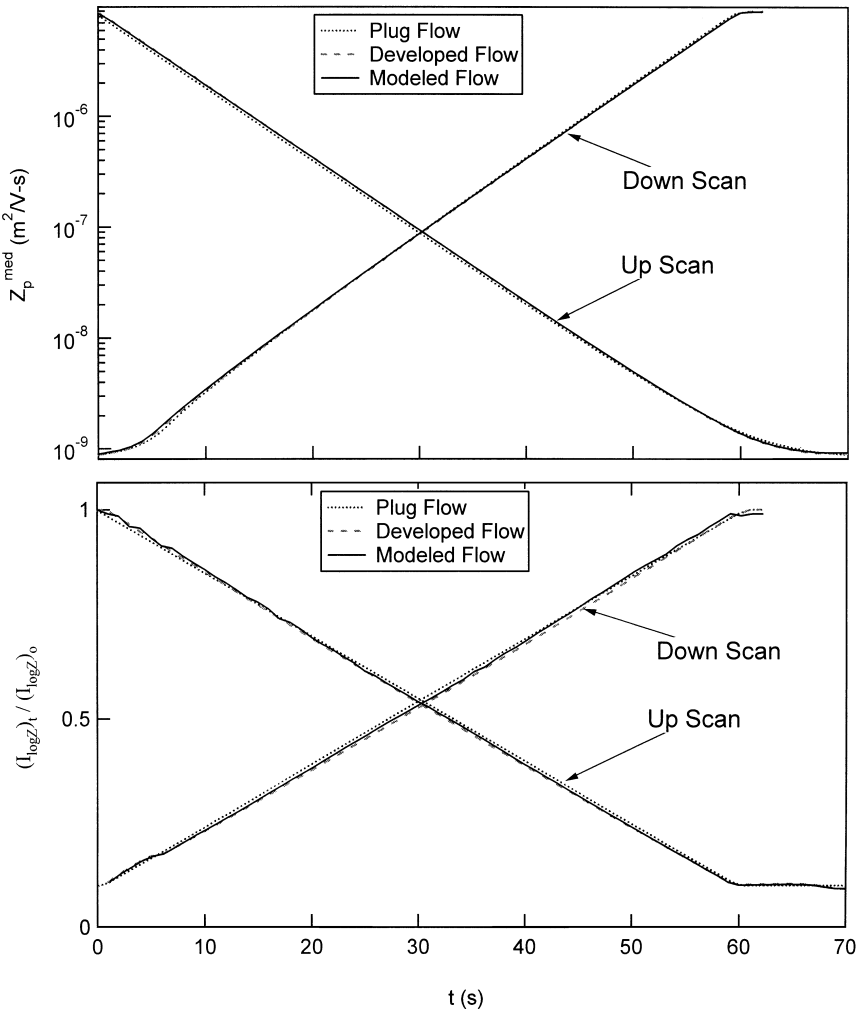

Fig. 4. Calculated Z_p^{med} and $I_{\log Z}$ for a 60 s scan during which the sheath flow was varied linearly from 2 to 20 L min^{-1} as the voltage was ramped from 10 to 10,000 V. Calculations were performed for plug flow, fully developed flow, and modeled flow.

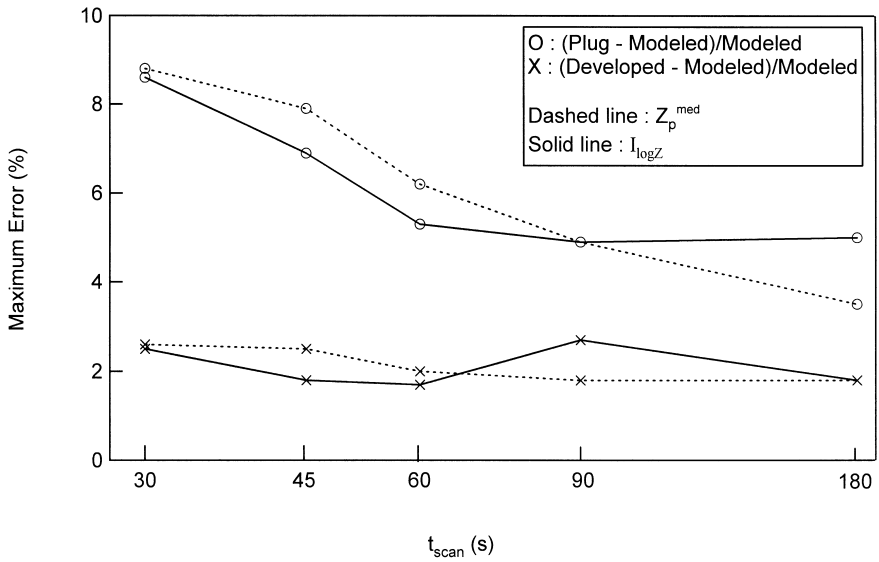

Fig. 5. Maximum error in the determination of the integral and median mobility of the transfer function from assuming either plug flow or fully developed flow within the DMA.

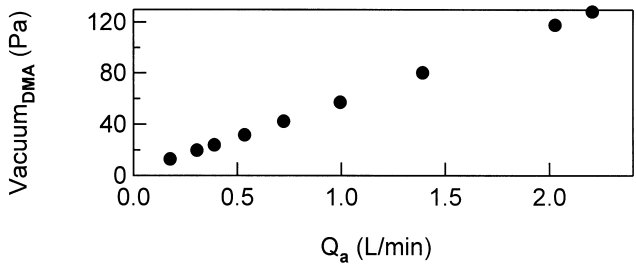

Fig. 6. Vacuum within the DMA due to the pressure drop associated with the aerosol flow.

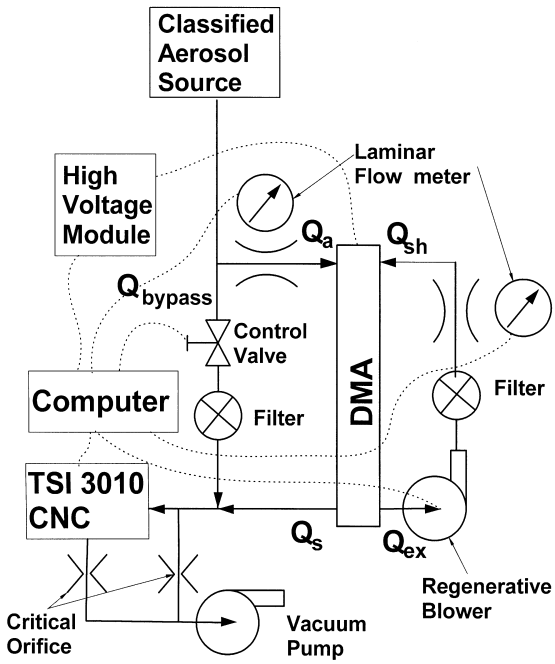

Fig. 7. Schematic of the experimental apparatus used.

a low volume recycle loop, so $Q_{sh} = Q_e$. Also, if the pressure within the recycle loop is directly related to the pressure within the DMA, it is the combined DMA/recycle loop volume that is relevant in equation (27). Applying the ideal gas law and assuming constant temperature yields a predicted flow imbalance between the sample and aerosol flows of

$$Q_a - Q_s = \frac{\mathscr{V}_{DMA}}{p}\frac{dp}{dt}. \tag{28}$$

Measurements of the DMA pressure as a function of aerosol flow rate are shown in Fig. 6. The combined volume of the DMA and recycle loop, $\mathscr{V}_{DMA}$, was approximately 1 L. For a one minute linear ramp in flow rate from 2 to 20 L min^{-1}, the deviation calculated using equation (28) between Q_s and Q_a is less than 1%. This discrepancy could become larger if the pressure drops within the DMA or the metering elements were larger, if the DMA volume were larger, of if a faster flow ramp were employed.

The experimental apparatus is illustrated in Fig. 7. In order to ensure that the sheath and excess flows are balanced as the flows are scanned, a closed loop recycle system (Wang *et al.*, 1992) was used. The variable recycle rate was facilitated by using a regenerative blower (EG&G Rotron HDC, SE12RE21). The regenerative blower is compact and lightweight,

and due to the low pressure operation, heats the gas less than the diaphragm pump used in the earlier implementation of sheath air recycle, reducing the risk of evaporating volatile aerosols in the course of measurement.† The aerosol flow was controlled by using a bypass flow that passed through a proportional solenoid valve (MKS 0248A-50000SV). The bypass flow was filtered and combined with the sample flow immediately after exiting the DMA so that the flow entering the TSI 3010 Condensation Particle Counter (CPC) remained constant in spite of the variable flows through the DMA. This not only facilitates the use of a particle detector or other in-line constant-flow apparatus, but also simplifies the final data analysis since the particle losses in the entrance and exit plumbing are constant and the plumbing time between the DMA and the CPC is only a weak function of the flow rates. All volumetric flow rates were measured using differential pressure transducers across laminar flow elements.

LabView (National Instruments) software was used to monitor all parameters and execute all control functions through a laboratory computer. Differential pressure transducer signals were measured and CPC pulses were counted using an A/D card (National Instruments PC-LPM-16), while a 12-bit D/A card (National Instruments AT-AO-6) was used to provide the control voltages to the regenerative blower, control valve, and a high voltage module. The wide dynamic range of the DMA voltage was accommodated by generating a signal proportional to the logarithm of the voltage and using an analog exponentiation circuit to drive the high voltage module (Bertan 602c-100). The control software was based on built-in proportional-integral-differential (PID) controller modules in the LabView software. The data were analyzed in real-time immediately following each scan with a recently developed data inversion routine that accounts for the smearing of the DMA response due to the residence time distribution of the CPC (Russell *et al*., 1995) and the DMA transfer function.

The performance of the scanning DMA was examined using a mobility classified aerosol. A nebulizer/diffusion dryer system was used to produce a polydisperse aerosol consisting of dry NaCl particles. The dried aerosol was processed through a mixing chamber with a mean residence time of approximately 5 min to minimize any fluctuations. A bipolar neutralizer containing 2 mCi of polonium-210 was used to neutralize the aerosol, and a cylindrical DMA identical to the one used for the scanning measurements was used for classification. This source aerosol was found to be extremely stable over a period of hours.

3. RESULTS AND DISCUSSION

For a given set of voltage and flow rate limitations associated with a DMA, there exists an infinite number of possible ramp combinations, several of which are examined below. Although the quantitative results presented are for the cylindrical DMA discussed above, the general trends and benefits described can be achieved with DMAs of any design, subject to the additional constraint that the range and rate of flow rates scanned not lead to flow instabilities.

The most obvious advantage of the flow-scanning mode of DMA operation is the extension of the range of particle sizes that can be accurately measured. Figure 8 compares the range of particle measurements that is attainable with a 10 to 10^4 V voltage scan with a constant sheath flow rate at an intermediate value of 5 L min^{-1} with that covered when the flow rate is decreased with time from 20 to 2 L min^{-1}. The minimum classified particle size decreases from 9.8 to 4.8 nm, while the maximum particle size increases from 537 to 1160 nm when flow scanning is implemented, extending the sizing range by a factor of 4.4. For a 60 s scan, this factor increases to 6.0 if only those particles that experience the exponential ramp are considered for the voltage-scanning method.

† It should be noted that for use in a closed loop such as this, the optional seal offered by EG&G Rotron is necessary to prevent leaks that will result in a flow imbalance.

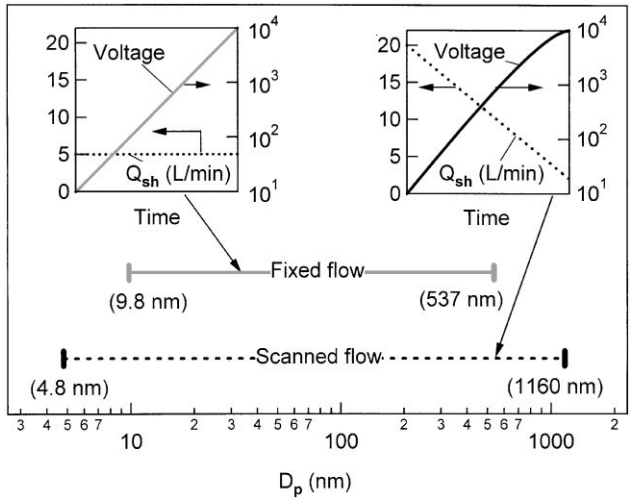

Fig. 8. Theoretical improvement in the measurable size range of a cylindrical DMA through the implementation of scanning flow rates. The fixed flow and scanning flow ramps used are shown as insets.

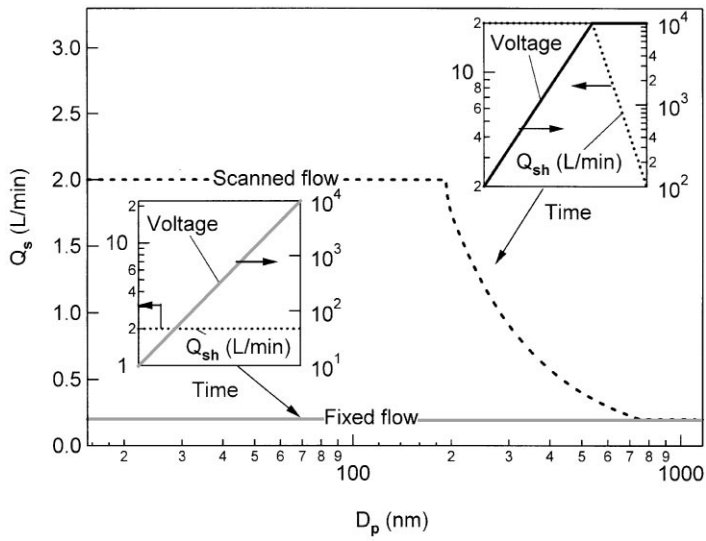

Fig. 9. Theoretical improvement in the monodisperse flow (and therefore counting statistics) through the implementation of scanning flow rates.

While improving the dynamic range of the DMA may be the most obvious benefit of flow scanning, it is by no means the only reason for adding this feature. If, as in the present work, the ratio of the aerosol to sheath flow rates is kept constant as the flow rate is scanned, an increase in the flow rate will increase the number of particles reaching the detector. In a clean environment, this can lead to substantial improvements in the uncertainties in number concentration measured. Consider measurements with a maximum size of 1 μm using the present cylindrical DMA. Given the breakdown potential of about 10,000 V, classification of these particles requires a flow rate of approximately 2 L min^{-1}. In scanning flow operation designed to maximize counting statistics, the flow rate at low voltage is increased by an order of magnitude, to 20 L min^{-1}, decreasing only when the particles can no longer be classified at this high flow rate as illustrated in Fig. 9. This results in a factor of $\sqrt{10}$ decrease in the uncertainty in the estimate of the particle concentration over a wide size range.

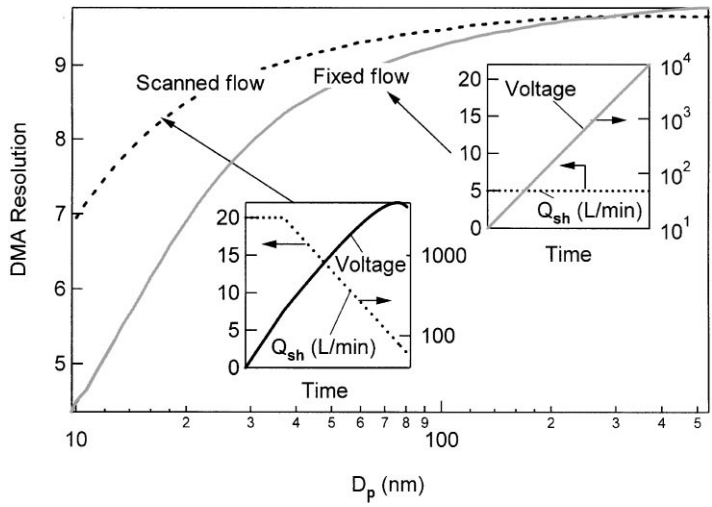

Fig. 10. Theoretical improvement in the limiting DMA resolution through the implementation of scanning flow rates.

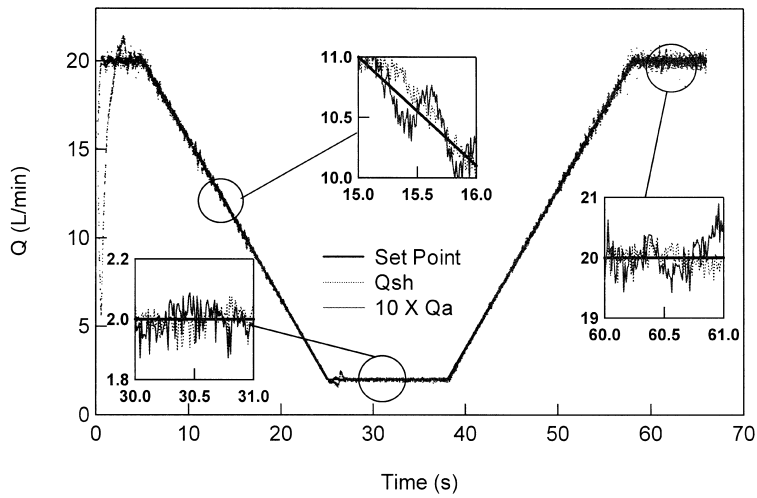

Fig. 11. Measured sheath and aerosol flow rates during a 20 s linear flow scan. The aerosol flow rate is multiplied by 10 to account for the aerosol to sheath flow ratio of 0.1.

The attainable resolution can also be dramatically enhanced by maximizing the classification voltage at every instant in the scan. Figure 10 presents a scan designed to increase resolution, while maximizing the flow scan time in order to facilitate accurate control. In this scan, the flow rate is first maintained at its maximum in order to allow the voltage to be increased as rapidly as possible. When a point is reached at which the resolution is deemed satisfactory, the flow rates begin their linear ramp, slowing the rate of change of the applied voltage. As indicated from calculations based on the Stolzenburg (1988) transfer function, the resolution for this scan profile is dramatically better than that of the conventional fixed flow rate operation, $Q_{sh} = 5\ \mathrm{L\,min^{-1}}$, over the same range of particle size. The resolution for the smallest particles classified is about 60% higher in the flow-scanning mode than when the voltage is scanned alone.

Experimental implementation of flow-scanning operation of the DMA requires that the flow rates accurately follow the prescribed time profile. The response of the DMA flows to the imposed ramp is shown in Fig. 11 for a 20 s ramp. A linear ramp has been employed here to facilitate flow control. The sheath flow rate and the aerosol flow rate (multiplied by $10 = \beta^{-1}$) are compared with the set point. The flow control was accurate and stable for this rate of change of the flows. Magnified regions of the profile show that the maximum

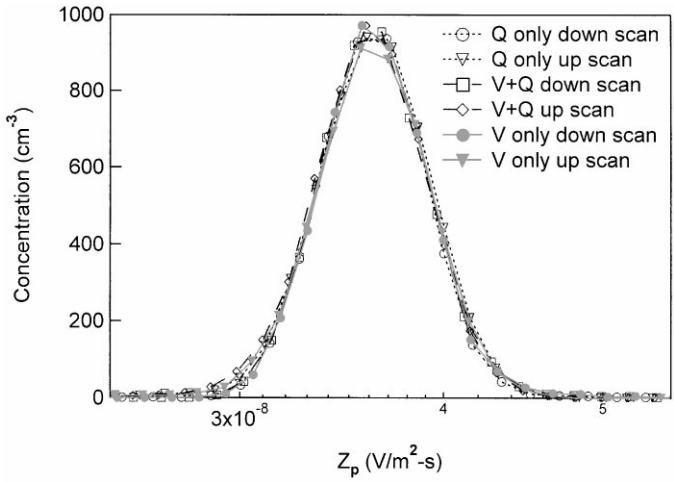

Fig. 12. Comparison of recovered mobility distributions obtained using a voltage ramp, a flow ramp, and a combined voltage and flow ramp. The ramp parameters used are listed in Table 1.

Table 1. Ramp parameters used for comparison between flow and voltage ramps

	V_{min} (V)	V_{max} (V)	Q_{min} (L min^{-1})	Q_{max} (L min^{-1})	t_{scan} (s)
V Scan	250	2500	5.0	5.0	60
$V + Q$ Scan	400	1200	2.5	8.0	60
Q Scan	750	750	2.0	20.0	60

deviation from the set point was less than 5% over the entire flow rate range. It is the average deviation over the residence time of the particles within the DMA ($\sim$ 1.1 to $\sim$ 11 s) that determines the uncertainty in the measured mobility, and this quantity is much smaller ($\sim$ 1%).

In order to examine the accuracy of the inverted distributions obtained using a flow ramp, a mobility classified aerosol was measured using a single DMA operated using three different ramps in succession. An exponential voltage ramp, an exponential flow ramp, and a coupled voltage/flow ramp are compared in Fig. 12. In order to compare the flow ramp directly with the voltage ramp, the range of mobilities scanned was limited to the range over which the flow rates could be accurately controlled. Therefore, each of the ramps scanned over approximately one order of magnitude in mobility during a 60 s scan, resulting in an exponential time constant of 26 s. The specific parameters for each of the ramps are listed in Table 1. Agreement between the different ramps is excellent, well within the expected experimental uncertainty.

Faster scans are required to measure rapidly changing aerosols or to achieve acceptable spatial resolution in measurements made aboard aircraft at high flight speeds. Figure 13 shows distributions recovered using flow scans of 30 and 60 s at constant voltage. Although slight deviations appear in the faster measurements, the errors introduced would be acceptable for many applications. As the flow scan time is decreased further, the recovered distributions retain the same mobility peak, but broaden somewhat. Flow irregularities may be responsible for a portion of this broadening, but factors unrelated to the flow ramp itself also contribute, most notably, the finite response time of the condensation nucleus counter. For the flow rate range used in these analyses, ramp times shorter than 10 to 15 s led to poor flow control and significant errors in the final distribution. Better recirculating pumps, control valves, and pressure transducers might alleviate some of this uncertainty.

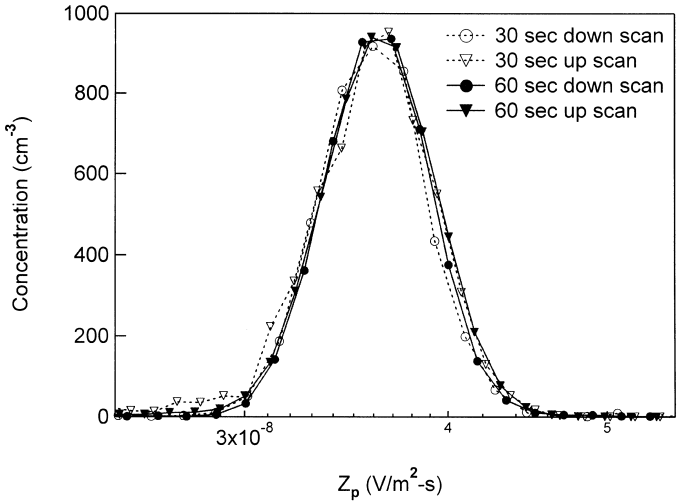

Fig. 13. Effect of decreasing the flow ramp time from 60 to 30 s. The sheath flow was ramped between 2 and 20 L min^{-1}.

4. SUMMARY

A DMA has been successfully operated with time-varied flow rates. Flow-scanning DMA measurements have several advantages over a DMA that relies only on voltage changes to scan across particle mobility. Constrained only by the requirements that laminar flow be maintained and electrostatic breakdown does not occur, optimization of the flow and voltage ramps can be used to increase the measurable size range, to improve counting statistics, or to enhance DMA resolution. However, unlike the voltage-scanning DMA, classified particles may follow different trajectories through the DMA, thereby complicating data analysis. The result is a trade-off between the benefits of flow scanning and the associated added uncertainties. Accurate control of the necessary flow rates over an order of magnitude range was accomplished for ramp times as small as 20 s. Excellent agreement was found between mobility distributions recovered from scans utilizing only a voltage ramp, scans utilizing only a flow ramp, and scans utilizing coordinated voltage and flow ramps. Slight deviations in the recovered distributions occur for flow ramp times of 30 s while more pronounced broadening occurs for ramps approaching the limitations of the flow control itself. These benefits require no modification to the DMA and can be achieved without significantly compromising the simplicity and reliability of a conventional DMA measurement system.

Acknowledgements—The authors gratefully acknowledge the assistance of Jian Wang, Patrick Chuang, and Jim Smith for their help in the construction and implementation of this measurement system. This work has been supported by the National Science Foundation Grant ATM-9614105, and by the Office of Naval Research Grant N00014-91-0119.

REFERENCES

Bird, R. B., Stewart, W. E. and Lightfoot, E. N. (1960) Transport Phenomena. Wiley, New York.

Brink, H. M. T., Plomp, A., Spoelstra, H. and van de Vate, J. F. (1983) A high resolution electrical mobility aerosol spectrometer (MAS). *J. Aerosol Sci.* **14,** 589–597.

de Juan, L. and de la Mora, J. F. (1998) High resolution size analysis of nanoparticles and ions: Running a Vienna DMA of near optimal length at Reynolds numbers up to 5000. *J. Aerosol Sci.* **29,** 617–626.

Fissan, H. J., Helsper, C. and Thielen, H. J. (1983) Determination of particle size distributions by means of an electrostatic classifier. *J. Aerosol Sci.* **14,** S354–S357.

Flagan, R. C. (1999) On differential mobility analyzer resolution. *Aerosol Sci. Technol.* **30,** 556–570.

Flagan, R. C., Wang, S. C., Yin, F. D., Seinfeld, J. H., Reischl, G., Winklmayr, W. and Karch, R. (1991) Electrical mobility measurements of fine-particle formation during chamber studies of atmospheric photochemical-reactions. *Environ. Sci. Technol.* **25,** 883–890.

Gosman, A. D. and Pun, W. M. (1974) Lecture Notes for 'Calculation of recirculating flows'. Imperial College, London.
Hansson, H. C. (1997). Personal communication.
Knutson, E. O. and Whitby, K. T. (1975) Aerosol classification by electric mobility: Apparatus, theory, and applications. *J. Aerosol Sci.* **6,** 443–451.
Meek, J. M. and Craggs, J.D. (Eds.) (1978) Electrical Breakdown of Gases. Wiley, New York.
Patankar, S. V. (1980). Numerical Heat Transfer and Fluid Flow. McGraw-Hill, New York.
Russell, L. M., Flagan, R. C. and Seinfeld, J. H. (1995) Asymmetric instrument response resulting from mixing effects in accelerated DMA-CPC measurements. *Aerosol Sci. Technol.* **23,** 491–509.
Russell, L. M., Zhang, S. H., Flagan, R. C., Seinfeld, J. H., Stolzenburg, M. R. and Caldow, R. (1996) Radially classified aerosol detector for aircraft-based submicron aerosol measurements. *J. Atmos. Ocean Technol.* **13**(3)**,** 598–609.
Stolzenburg, M. R. (1988). An ultrafine aerosol size distribution measuring system. Ph.D. thesis, University of Minnesota.
Wang, S. C. and Flagan, R. C. (1989) Scanning electrical mobility spectrometer. *J. Aerosol Sci.* **20,** 1485–1488.
Wang, S. C., Paulson, S. E., Grosjean, D., Flagan, R. C. and Seinfeld, J. H. (1992) Aerosol formation and growth in atmospheric organic NOX systems .1. outdoor smog chamber studies of C-7-hydrocarbons and C-8-hydrocarbons. *Atmos. Envir.* **26,** 403–420.
Zhang, S. H., Akutsu, Y., Russell, L. M., Flagan, R. C. and Seinfeld, J. H. (1995) Radial differential mobility analyzer. *Aerosol Sci. Technol.* **23,** 357–372.